Quantum Hall plateau transition in the lowest Landau level of disordered graphene

Pallab Goswami, Xun Jia, and Sudip Chakravarty
Department of Physics and Astronomy, University of California Los Angeles, Los Angeles, California 90095-1547, USA
(Received 9 July 2007; published 8 November 2007)

We investigate, analytically and numerically, the effects of disorder on the density of states and on the localization properties of relativistic two-dimensional fermions in the lowest Landau level. Employing a supersymmetric technique, we calculate the exact density of states for the Cauchy (Lorentzian) distribution for various types of disorder. We use a numerical technique to establish the localization-delocalization (LD) transition in the lowest Landau level. For some types of disorder, the LD transition is shown to belong to a different universality class, as compared to the corresponding nonrelativistic problem. The results are relevant to the integer quantum Hall plateau transitions observed in graphene.

DOI: 10.1103/PhysRevB.76.205408 PACS number(s): 73.43.−f, 73.43.Nq, 71.30.+h, 72.15.Rn

I. INTRODUCTION

Recent experiments[1] have unraveled a fascinating set of phenomena in the atomically thin layer of hexagonally arranged carbon atoms known as graphene.[2] The quasiparticles of graphene are (2+1)-dimensional massless Weyl fermions.[3,4] In the context of condensed matter physics, their properties are strikingly different from those of nonrelativistic fermions; and phenomena that are hard to realize for the relativistic case, such as the Klein paradox or the *Zitterbewegung*, are accessible in graphene.[5] It is perhaps not an exaggeration to remark that many subtleties and a rich set of phenomenology are waiting to be discovered.

A. Quantum Hall effect

A highlight has been the observation of an unconventional quantum Hall effect[6–8] and the corresponding theoretical development.[9–18] In graphene the filling fractions are $\nu_f = \pm 4\left(n+\frac{1}{2}\right)$ for magnetic field $B<9$ T, where n is an integer.[6–8] The factor of 4 comes from the twofold spin degeneracy and the twofold nodal degeneracy of the Landau levels. The Zeeman splitting is negligible compared to the cyclotron frequency and the disorder broadening of the Landau levels. The factor of $1/2$ is due to a zero mode in the Landau level spectrum of Dirac fermions.[9–11]

For stronger magnetic fields, $20<B<45$ T, plateaus appear at $\nu_f=0,\pm 1,\pm 2q$, where q is an integer.[8] The plateaus at $\nu_f=0,\pm 1$ can be explained by the lifting of both the spin and the nodal degeneracies in the lowest Landau level (LLL), but those at $\nu_f=\pm 4,\pm 6,\ldots$ reflect only the removal of spin degeneracy in higher Landau levels. The removal of nodal degeneracy requires electron-electron interaction. Mechanisms suggested include SU(4) ferromagnetism,[14,15] sublattice symmetry breaking due to short-range interactions,[16] and the generation of a mass gap by magnetic catalysis.[17–19] SU(4) quantum Hall ferromagnetism predicts plateaus at all odd integer filling fractions. However, apart from $\nu_f=\pm 1$, the plateaus at $\nu_f=\pm 3,\pm 5,\ldots$ have not yet been observed.

B. Localization-delocalization transition

The special quantization rules in graphene are explained by the relativistic Landau levels, modified perhaps by interactions, but for the existence of Hall plateaus the Laughlin argument is necessary.[20] According to this argument, the extended states at the center of a Landau band are separated by the localized states elsewhere. If the Fermi energy falls in the mobility gap, the plateaus are explained by a gauge invariance argument that is remarkably robust. The underlying phenomenon, therefore, is a localization-delocalization (LD) transition at the band center.[20–23] The conventional integer quantum Hall (IQH) plateau transition has been widely studied, and it is known that the localization length exponent $\nu \approx \frac{7}{3}$.[24–31] Can we prove that the same argument applies to graphene, and, if so, does the LD transition belong to the same universality class?

C. Disorder and Dirac fermions

In the absence of a magnetic field, Dirac fermions in the presence of disorder have been widely studied in systems as varied as gapless semiconductors,[32] gapless superconductors,[33,34] and IQH plateau transitions.[35,36] As compared to nonrelativistic fermions, the localization problem of Dirac fermions is richer because of a number of discrete symmetries. More specifically, if the disorder is particle-hole symmetric, for example a random gauge field, the LD transition takes place at zero energy and is reflected in the single-particle density of states (DOS), in contrast to the conventional metal-insulator transition where the DOS is smooth through the LD transition. Surprisingly, there is a line of fixed points with continuously varying exponents depending on the disorder coupling constant.[33,34,36–38] Some of the unusual behaviors of disordered Dirac fermions may be expected to be realized in graphene. One such effect that has received considerable attention is the weak (anti)localization phenomenon.[39–44] However, relativistic Landau levels in the presence of disorder have not yet received much attention.[11,45–48] Here we provide a reasonably complete study of the possible effects.

There is another important reason why LD transitions in the relativistic Landau level should be carefully analyzed. In the conventional IQH effect, the spin-degenerate plateau transition corresponds to $\nu \sim 4.6$ when it is assumed that the LD transition takes place at a single energy at the band center.[49–52] This has led to intense theoretical investigation of

the LD transition in the spin-degenerate Landau band.[53–57] When spin-orbit scattering is included, the LD transition is found to occur at two distinct energies, away from the band center. Scaling analysis about these distinct energies shows, once again, that $\nu \approx 7/3$, as in the spin-polarized system. The scaling about a single energy at the band center leads to the effective exponent $\nu \sim 4.6$. One should anticipate a similar discrepancy between the spin- and the nodal-polarized IQH effect and the fourfold-degenerate IQH effect in graphene.

D. Graphene in the lowest Landau level

For simplicity we shall concentrate on the spin-polarized lowest Landau level of graphene and analyze the LD transition both in the presence and in the absence of nodal degeneracy. An interesting example of a controlled analytic calculation in the disordered Landau level problem is the DOS in the LLL. This was first computed exactly by Wegner[58] by examining the Euler trails of the impurity diagrams for white noise disorder and was subsequently extended by Brezin *et al.*[59] by using a supersymmetric (SUSY) technique. Here we also obtain some exact results for the DOS in the disordered relativistic LLL using SUSY techniques.

The most general model of disorder consists of a random potential, a random mass, a random gauge field, and a random internode scattering; however, the random gauge field leaves the LLL unperturbed. After projection to the spin-polarized LLL, we study the following Hamiltonian:

$$\hat{H}_{\mathrm{LLL}} = m\eta_3 + \sum_{j=0}^{3} V_j(\vec{r})\eta_j, \tag{1}$$

where $V_0(\vec{r})$ and $V_3(\vec{r})$ represent potential and mass disorders, respectively, and $V_1(\vec{r})$ and $V_2(\vec{r})$ describe internode scattering effects. The mass m of the fermions has been included to study the effect of the removal of the nodal degeneracy. For simplicity we have omitted the constant Zeeman energy. The 2×2 matrix η_0 is the identity matrix and η_1, η_2, and η_3 are the three Pauli matrices.

E. Summary of results

Because of the large number of cases involved, it is useful to summarize the results for the LD transition. Let g_0, g_3, g_1, and g_2 denote the widths of the Gaussian random distributions corresponding to the random potential, random mass, and random internode scatterings, respectively.

1. $m=0$

The list of possible cases is as follows. (1) $g_0\neq 0$, $g_3=g_1=g_2=0$; (2) $g_3\neq 0$, $g_0=g_1=g_2=0$; (3) $g_2\neq 0$, $g_0=g_3=g_1=0$; (4) $g_1\neq 0$, $g_0=g_3=g_2=0$; (5) $g_0\neq 0$, $g_3\neq 0$, $g_1=g_2=0$; (6) $g_0\neq 0$, $g_2\neq 0$, $g_3=g_1=0$; (7) $g_0\neq 0$, $g_1\neq 0$, $g_3=g_2=0$; (8) $g_3\neq 0$, $g_2\neq 0$, $g_0=g_1=0$; (9) $g_3\neq 0$, $g_1\neq 0$, $g_0=g_2=0$; (10) $g_2\neq 0$, $g_1\neq 0$, $g_0=g_3=0$; (11) $g_0\neq 0$, $g_3\neq 0$, $g_2\neq 0$, $g_1=0$; (12) $g_0\neq 0$, $g_3\neq 0$, $g_1\neq 0$, $g_2=0$; (13) $g_0\neq 0$, $g_2\neq 0$, $g_1\neq 0$, $g_3=0$; (14) $g_3\neq 0$, $g_2\neq 0$, $g_1\neq 0$, $g_0=0$; and (15) $g_0\neq 0$, $g_3\neq 0$, $g_2\neq 0$, $g_1\neq 0$.

In the cases 1 and 2, when disorder does not mix the two nodes, the LD transitions belong to the conventional IQH universality class with $\nu \approx 7/3$. It is interesting to note that mass disorder produces a LD transition in the LLL, whereas for zero magnetic field random mass is known to be an irrelevant perturbation for the $(2+1)$-dimensional Dirac fermions.[36] The Hamiltonians for cases 2, 3, and 4 involve only a single Pauli matrix at a time, related to each other by unitary transformations. Thus, cases 2, 3, and 4 are equivalent to each other and have $\nu \approx 7/3$. Because unitary transformations leave the identity matrix invariant, the same argument implies that cases 5, 6, and 7 are equivalent to each other and once again $\nu \approx 7/3$.

Cases 8, 9, and 10 involve a pair of Pauli matrices and are equivalent to each other. In case 8 the Hamiltonian has a discrete symmetry $\eta_1 H \eta_1 = -H$, often called particle-hole symmetry. Cases 9 and 10 have the same discrete symmetry with respect to η_2 and η_3. Case 10 has been analyzed by Hikami *et al.*[60] for a spin-degenerate nonrelativistic LLL. When $g_1=g_2$, the DOS diverges at the band center and has two symmetrically located peaks away from it. The LD transition takes place at these three distinct energies. Away from the band center the LD transition has the exponent $\nu \sim 2.98$ and the transition at the band center corresponds to a different exponent. If $g_1 \neq g_2$, the divergence of the DOS at the band center disappears, but the two symmetrically placed peaks away from the band center still exist. We find that the LD transitions at these two energies have continuously varying exponents depending on the ratio g_2/g_1.

Cases 11, 12, and 13 are equivalent. The Hamiltonians in these cases are, respectively, the Hamiltonians for cases 8, 9, and 10, augmented by the identity matrix corresponding to the potential disorder. Potential disorder breaks the discrete symmetry mentioned above, and there is no divergence of the DOS at the band center. The DOS is still peaked at two symmetrically placed energies away from the band center. The LD transitions occur at energies away from the band center. If g_0 is much smaller than the two remaining coupling constants, ν follows trends similar to those in cases 8, 9, and 10. If g_0 is comparable or larger, we find $\nu \sim 7/3$.

In case 14 all three Pauli matrices are present. The discrete symmetry of cases 8, 9, and 10 are absent, and the LD transitions take place at two symmetrically placed energies away from the band center. When all the coupling constants are equal, the exponent $\nu \sim 3.6$. Depending on the relative strengths of the coupling constants, the exponents vary continuously. If any particular coupling constant is significantly larger than the rest, $\nu \sim 7/3$. By adding g_0 we obtain case 15. If g_0 is smaller than the rest, the situation is similar to case 14. If g_0 is larger than the rest, $\nu \sim 7/3$.

2. $m\neq 0$

When $m\neq 0$, the LD transitions occur at two symmetrically placed energies about the band center, and these energies are greater than or equal to m. In the absence of internode scattering, the transitions occur at $E=\pm m$ and the exponent $\nu \sim 7/3$. If the strength of the intranode scattering is larger than m, the bands at $\pm m$ overlap and effectively correspond to the nodally degenerate case.

If $g_0=g_3=0$ and only one of the internode couplings is present, the DOS diverges at $E=\pm m$ with an exponent of 0.5 and is identically zero for $|E|<m$. The LD transitions occur at $E=\pm m$ and have a continuously varying exponent. When the disorder is strong compared to m, $\nu\sim 7/3$, and, in the opposite limit, ν approaches unity. If we include small intranode scattering the situation is similar. If the intranode scattering strength is greater than the internode scattering, $\nu\sim 7/3$.

When $g_0=g_3=0$ and both internode couplings are present, the DOS diverges at $E=\pm m$ with an exponent $\nu\sim 0.47$. However, the LD transitions occur at energies larger than $|m|$. We have analyzed the case where $g_1=g_2$. The exponent varies continuously. If the internode scattering strength is larger than m, $\nu\sim 3.8$, and in the opposite limit ν approaches unity. This behavior is stable against intranode scattering if its strength is smaller than both m and the internode scattering. If the intranode scattering strength is larger than the internode scattering, $\nu\sim 7/3$.

F. Road map

Our paper is organized as follows: In Sec. II we describe the Dirac fermion model. In Sec. III we describe various possible disorders and their forms when projected to the LLL. In Sec. IV we calculate the averaged density of states using supersymmetry. In Secs. V–VII we describe the numerical studies of the LD transition projected to the lowest Landau level. Section VIII is a brief concluding section. In Appendix A we provide some mathematical details of the density of states calculation. In Appendix B we describe the recursive Green function technique used for numerical calculations, and finally in Appendix C we outline the procedure of data collapse involved in the finite-size scaling of the localization length.

II. DIRAC FERMIONS AND LANDAU LEVELS OF GRAPHENE

The low-energy quasiparticles in graphene are well described by the Lorentz-invariant form as the sum over two inequivalent nodes (the Fermi velocity $v_F\approx 10^6$ m/s)

$$H_0=-i\hbar v_F\int d^2r\,\bar{\Psi}_\sigma(\gamma^1 D_x+\gamma^2 D_y)\Psi_\sigma, \tag{2}$$

where $\bar{\Psi}_\sigma=\Psi_\sigma^\dagger\gamma^0$ and the summation over spin $\sigma=\pm 1$ is understood. The four-component Dirac spinor $\Psi_\sigma^\dagger=(\psi_{KA\sigma}^\dagger,\psi_{KB\sigma}^\dagger,i\psi_{K'B\sigma}^\dagger,-i\psi_{K'A\sigma}^\dagger)$, where the component $\psi_{KA\sigma}$ is constructed by superposing Bloch functions close to one of the two inequivalent nodes (K,K') of the Brillouin zone, corresponding to one of the two sublattices (A,B) of the hexagonal graphene lattice. The notation $\mathbf{D}=[\boldsymbol{\partial}-i(e/c)\mathbf{A}]$ stands for the covariant derivative, $\mathbf{A}$ being the vector potential. The γ matrices are defined by $\gamma^\mu=(\tau_3,i\tau_1,i\tau_2)\otimes\eta_3$; the Pauli matrix τ operates on the two components corresponding to the sublattice indices, and the Pauli matrix η operates on the components corresponding to the nodal indices. To be explicit,

$$\gamma^0=\begin{pmatrix}\tau_3 & 0\\ 0 & -\tau_3\end{pmatrix},\quad \gamma^1=\begin{pmatrix}i\tau_1 & 0\\ 0 & -i\tau_1\end{pmatrix},\quad \gamma^2=\begin{pmatrix}i\tau_2 & 0\\ 0 & -i\tau_2\end{pmatrix}. \tag{3}$$

To include a Zeeman term, we add

$$H_z=E_z\int d^2r\,\bar{\Psi}_\sigma\gamma^0\sigma_3^{\sigma\sigma'}\Psi_{\sigma'}, \tag{4}$$

where $E_z=g\mu_B B$ is the Zeeman energy and σ_j is a Pauli matrix operating on the spin indices. The Zeeman term breaks the SU(2) symmetry of the spin space down to U(1). The energy eigenvalues of the Hamiltonian operator

$$\hat{H}_0=-i\hbar v_F\gamma^0(\gamma^1 D_x+\gamma^2 D_y)+E_z\sigma_3 \tag{5}$$

are well known:

$$E_{ns\sigma}=s\sqrt{2n|eB|\hbar v_F^2/c}-\sigma E_z,\quad n=1,2,\ldots, \tag{6}$$

$$E_{n=0,\sigma}=-\sigma E_z, \tag{7}$$

where $s=\pm 1$ refer to the particle and the hole branches. In the presence of disorder, the Landau levels get broadened into a band, and the amount of broadening depends on the strength of the disorder. When the disorder is very strong, the half-width of the broadened band can be larger than E_z, and experimentally this corresponds to the spin degeneracy of the Landau bands. In the spin-degenerate situation, the observed filling factor is given by $\nu_f=4(n+\frac{1}{2})$.[9,10]

The LLL wave function in the absence of disorder in the symmetric gauge $\mathbf{A}=(-By/2,Bx/2,0)$ can be written as

$$\mathcal{U}(z,\bar{z})=e^{-z\bar{z}/4l_B^2}\begin{pmatrix}f_1(z)\\ 0\\ f_2(z)\\ 0\end{pmatrix}, \tag{8}$$

where $eB>0$. The functions $f_1(z)$ and $f_2(z)$ are holomorphic functions of the complex coordinates $z=x+iy$, $\bar{z}=x-iy$, and $l_B=\sqrt{\hbar c/|eB|}$ is the magnetic length. Hence, in the zero mode, the first and the second nodes have nonzero amplitudes coming only from the sublattices A and B, respectively.

Two distinct on-site energies on the two sublattices correspond to a charge density modulation at the lattice scale. As a result, the particle and hole branches acquire an energy gap. When linearized about the inequivalent nodes, this energy gap appears as a parity-preserving mass of the Dirac fermions. To be explicit, the linearized Hamiltonian will have two new terms: the chemical potential term $[(V_A+V_B)/2]\bar{\Psi}\gamma^0\Psi$ and the mass term $[(V_A-V_B)/2]\bar{\Psi}\Psi$, where V_A and V_B are the site energies at the sublattices A and B.

Although the noninteracting quasiparticles are massless in the absence of site modulation, they can acquire a parity-conserving mass due to interaction effects. This spontaneous symmetry breaking is facilitated by the presence of the magnetic field, a phenomenon known as "magnetic catalysis" of chiral symmetry breaking.[61,62] The effect has been argued to be the reason for quantum Hall plateaus at $\nu_f=0,\pm 1$ observed in strong magnetic fields.[17,18] Though it is beyond the

scope of the present paper to consider electronic interactions, we will pay some attention to the noninteracting problem with a finite mass. Our philosophy is to analyze the consequences of having a mass (possible in an interacting theory) on the LD transition. So we shall include the term $m\Psi^\dagger\gamma^0\Psi$ in the effective Hamiltonian to examine the effect of mass. In the presence of such a mass term, the nodal degeneracy of $E_{n=0,\sigma}=-\sigma E_z$ is removed and it splits into four levels: $\pm m - \sigma E_z$. Each of these levels has the degeneracy $|eB|/2\pi\hbar c$. If the applied chemical potential is smaller than $|E_z-m|$, there will be a plateau at $\nu_f=0$. If $|E_z-m|<|\mu|<E_z+m$, $\nu_f=\pm 1$ plateaus will appear depending on the sign of μ.[16,61] The next possible values of the quantized plateaus are $\nu_f=\pm 2$. The introduction of the mass term does not, however, lift the nodal degeneracy of the higher Landau levels, and the energy levels $E_{n\geq 1,s,\sigma}=s\sqrt{m^2+2n|eB|\hbar v_F^2/c}-\sigma E_z$ have the degeneracy $|eB|/\pi\hbar c$. Therefore, when a mass is included, quantized plateaus appear at $\nu_f=0,\pm 1,\pm 2q$, where q is an integer.

III. RANDOMNESS

There are many sources of disorder in graphene: vacancies, interstitials, substrate disorder, and lattice distortions due to dislocations. In principle, there could also be random spin-orbit coupling. However, due to the small atomic mass of carbon, spin-orbit coupling is very weak compared to other energy scales. For simplicity, we shall primarily be interested in the spin-polarized limit and ignore the random spin-orbit coupling.

Point defects and substrate disorder can be described by introducing random site energies in the tight-binding model. In the presence of substrate disorder there can also be a random modulation of the charge densities between the two sublattices. These effects can be described by a random chemical potential $V_0(\mathbf{r})\bar{\Psi}\gamma^0\Psi$ and a random mass $V_3(\mathbf{r})\bar{\Psi}\Psi$ in the continuum limit.

Because true long-range crystalline order is not possible in two dimensions at any finite temperature, topological defects, dislocations, and disclinations will be present. The effects of these topological defects will result in random hopping amplitudes δt_{AB}, and hence intranode as well as internode scattering. However, these scattering processes will take place between states on different sublattices. The two bilinears $V_2(\mathbf{r})\bar{\Psi}\gamma^3\Psi$ and $V_1(\mathbf{r})\bar{\Psi}\gamma^5\Psi$ describe the internode scattering terms arising from random hopping. The two mutually anticommuting matrices

$$\gamma^3 = i\begin{pmatrix} 0 & I \\ I & 0 \end{pmatrix}, \quad \gamma^5 = \begin{pmatrix} 0 & -I \\ I & 0 \end{pmatrix} \tag{9}$$

also anticommute with γ^μ; I is the identity matrix.

In the continuum limit, the most general impurity Hamiltonian is a 4×4 matrix:

$$H^{\text{imp}} = \int d^2r\, \Psi_\sigma^\dagger \begin{pmatrix} D_{11}(\mathbf{r}) & D_{12}(\mathbf{r}) \\ D_{21}(\mathbf{r}) & D_{22}(\mathbf{r}) \end{pmatrix} \Psi_\sigma, \tag{10}$$

where $D_{ij}(\mathbf{r})$ are 2×2 matrices. Here $D_{11}=D_{11}^\dagger$ and $D_{22}=D_{22}^\dagger$ represent intranode scattering at nodes 1 and 2, respectively; $D_{12}=D_{21}^\dagger$ represent internode scattering.

After projecting to the LLL, the disorder matrix reduces to a 2×2 matrix and can be represented by the Pauli matrices η. The most general disorder matrix projected to the LLL then takes the form

$$\hat{H}_{\text{LLL}}^{\text{imp}} = \sum_{j=0}^{3} V_j(\vec{r})\,\eta_j, \tag{11}$$

where we have denoted the I matrix by η_0.

IV. AVERAGE DENSITY OF STATES

Using a four-component bosonic spinor ϕ and a four-component Grassmann spinor χ, the average retarded Green function for a noninteracting problem can be written as

$$\bar{G}^R(E;r,r') = -i\prod_{j=0}^{3}\int \mathcal{D}[\phi^*]\mathcal{D}[\phi]\mathcal{D}[\chi^*]\mathcal{D}[\chi] \times \mathcal{D}[V_j]P[V_j]\phi^*(r)\phi(r')e^{S^R}, \tag{12}$$

where $P[V_j]$ is the probability distribution of V_j and

$$S^R = i\int d^2r[\phi^\dagger(E-\hat{H}_0-\hat{H}^{\text{imp}}+i\delta)\phi + \chi^\dagger(E-\hat{H}_0-\hat{H}^{\text{imp}}+i\delta)\chi]. \tag{13}$$

The average density of states is given by

$$\bar{\rho}(E) = -\frac{1}{\pi}\,\text{Im}\,\bar{G}^R(E;r,r). \tag{14}$$

After performing the disorder averages, we can write

$$\bar{G}^R(E;r,r') = -i\int \mathcal{D}[\phi^*]\mathcal{D}[\phi]\mathcal{D}[\chi^*]\mathcal{D}[\chi]\phi^*(r)\phi(r')e^{\mathcal{A}^R}, \tag{15}$$

where the action $\mathcal{A}^R$ involves interactions among the fields generated by the disorder averaging procedure. After projection to the LLL, the action $\mathcal{A}^R$ can be expressed in terms of a two-component holomorphic bosonic spinor

$$\phi(z) = \begin{pmatrix} v_1(z) \\ v_2(z) \end{pmatrix} \tag{16}$$

and a two-component holomorphic Grassmann spinor

$$\chi(z) = \begin{pmatrix} w_1(z) \\ w_2(z) \end{pmatrix}. \tag{17}$$

In terms of these fields the action is given by

$$\mathcal{A}^R = \mathcal{A}_f^R + \sum_{j=0}^{3}\mathcal{A}_j^D,$$

$$\mathcal{A}_f^R = i\epsilon\int d^2z\, e^{-z\bar{z}/2l_B^2}(\phi^\dagger\phi+\chi^\dagger\chi),$$

$$\mathcal{A}_j^D = \int d^2z\, h_j[e^{-z\bar{z}/2l_B^2}(\phi^\dagger \eta_j \phi + \chi^\dagger \eta_j \chi)], \tag{18}$$

where $\epsilon = E + i\delta$ and

$$h_j(\kappa) = \ln\left(\int e^{-i\kappa V_j} P[V_j]\mathcal{D}V_j\right) \tag{19}$$

is the effective interaction of the fields generated by averaging over the random variable V_j. For the Cauchy distribution, defined by

$$P[V_j(\vec{r})] = \frac{g_j}{\pi}\frac{1}{g_j^2 + V_j^2(\vec{r})}, \tag{20}$$

we have

$$h_j(\kappa) = -g_j|\kappa|. \tag{21}$$

If the disorder distribution is Gaussian white noise, defined by

$$P[V_j(\vec{r})] = \mathcal{N}\exp\left(-\frac{1}{2g_j}\int d^2r\, V_j^2(\vec{r})\right), \tag{22}$$

we get

$$h_j(\kappa) = -\frac{1}{2}g_j\kappa^2. \tag{23}$$

The above action is invariant under translation followed by a gauge transformation. Due to this invariance, the spatial dependence of the average retarded Green function is the same as the spatial dependence of the pure system's Green function,

$$G^R_{\text{pure}}(E, z_1, z_2) = \frac{\exp[-(|z_1|^2 + |z_2|^2) - 2z_1\bar{z}_2]}{2\pi l_B^2(E + i\delta)}. \tag{24}$$

The disorder-averaged Green function can be written as

$$\bar{G}^R(E, z_1, z_2) = C(E + i\delta, g_j)\exp[-(|z_1|^2 + |z_2|^2) - 2z_1\bar{z}_2], \tag{25}$$

where the g_j's are coupling constants of various types of disorder and $C(E+i\delta, g_j)$ is a gauge-invariant proportionality constant which depends on the energy and disorder strengths. This gauge-invariant proportionality constant is what we need to calculate to find the average density of states.

For the calculation of the average Green function's dependence on the energy and disorder coupling constants, we introduce two new Grassmann variables θ and $\bar{\theta}$ and enlarge the Euclidean coordinate space into a superspace of coordinates $(x, y, \theta, \bar{\theta})$. Integrals over the Grassmann coordinates are normalized as $\pi\int d\theta\, d\bar{\theta}\, \bar{\theta}\theta = 1$. The norm of a coordinate vector is defined as $x^2 + y^2 + \bar{\theta}\theta$. This norm is invariant under superspace rotations. In addition to the ordinary rotations in the Euclidean subspace and the symplectic transformations in the Grassmann subspace, the superspace rotations involve transformations that mix (x, y) and $(\theta, \bar{\theta})$ in the following manner:

$$\vec{r} \to \vec{r} + 2\vec{l}_1\Omega\theta + 2\vec{l}_2\Omega\bar{\theta},$$

$$\theta \to \theta + 4(\vec{l}_2 \cdot \vec{r})\Omega, \quad \bar{\theta} \to \bar{\theta} - 4(\vec{l}_1 \cdot \vec{r})\Omega. \tag{26}$$

In the above set of transformations $\vec{l}_{1,2}$ are two arbitrary Euclidean vectors and Ω is a Grassmann number. We also define two holomorphic superfields and their conjugates as

$$\Phi(z, \theta) = \phi(z) + \frac{\theta}{\sqrt{2}l_B}\chi(z),$$

$$\bar{\Phi}(z, \theta) = \phi^\dagger(z) + \frac{\chi^\dagger(z)}{\sqrt{2}l_B}\bar{\theta}. \tag{27}$$

In terms of these superfields the pure part of the action can be expressed as

$$\mathcal{A}_f^R = 2i\epsilon\pi l_B^2 \int d^2z\, d\theta\, d\bar{\theta}\, e^{-(z\bar{z}+\theta\bar{\theta})/2l_B^2}\bar{\Phi}\Phi, \tag{28}$$

which is manifestly invariant under superspace rotations. After the disorder contributions to the action are expressed in terms of these new superfields, we have to demonstrate these to be invariant under superspace rotations. In order to be supersymmetric, the $\mathcal{A}_j^D$'s have to be local in the supercoordinate space and this is possible only if they do not involve any quartic fermionic interactions. We note that

$$\begin{aligned} h_j[e^{-z\bar{z}/2l_B^2}(\phi^\dagger \eta_j \phi + \chi^\dagger \eta_j \chi)] &= h_j(e^{-z\bar{z}/2l_B^2}\phi^\dagger \eta_j \phi) + h_j'(e^{-z\bar{z}/2l_B^2}\phi^\dagger \eta_j \phi)e^{-z\bar{z}/2l_B^2}\chi^\dagger \eta_j \chi \\ &\quad + \frac{1}{2}h_j''(e^{-z\bar{z}/2l_B^2}\phi^\dagger \eta_j \phi)e^{-z\bar{z}/l_B^2}(\chi^\dagger \eta_j \chi)^2, \end{aligned} \tag{29}$$

where h_j' and h_j'' correspond to the first and second derivatives of h_j with respect to its argument. The Taylor series truncates at the quadratic order as the higher powers of $\chi^\dagger \eta_j \chi$ are identically zero according to the anticommutation rules. We also note that $(\chi^\dagger \eta_j \chi)^2 = -2w_1^\dagger w_1 w_2^\dagger w_2$ for $j = 1, 2, 3$ and $(\chi^\dagger \eta_0 \chi)^2 = 2w_1^\dagger w_1 w_2^\dagger w_2$. If h_j'' does not vanish, we get four-fermion interactions.

If there were one bosonic and one Grassmann field instead of spinors, as in the problem solved by Brézin *et al.*,[59] no four-fermionic terms would be generated, and the action for an arbitrary disorder distribution would be local in the superspace coordinates. For the case under consideration, such a simplification is not possible in general. However, for a Cauchy distribution the disorder-averaged action is quadratic and can be made manifestly supersymmetric. Thus, the calculation of the DOS reduces to a calculation of a zero-dimensional field theory over two complex bosonic fields.

A. Cauchy distribution

1. $m=0$

The action is given by

$$\mathcal{A}^R = \int d^2z\, e^{-z\bar{z}/2l_B^2}\left(i\epsilon(\phi^\dagger\phi + \chi^\dagger\chi) - \sum_{j=0}^{3} g_j|\phi^\dagger\eta_j\phi + \chi^\dagger\eta_j\chi|\right). \tag{30}$$

Using the superfields Φ and $\bar{\Phi}$, the action can be written as

$$\mathcal{A}^R = 2\pi l_B^2 \int d^2z\, d\theta\, d\bar{\theta}\, e^{-(z\bar{z}+\theta\bar{\theta})/2l_B^2}\left(i\epsilon\bar{\Phi}\Phi - \sum_{j=0}^{3} g_j|\bar{\Phi}\eta_j\Phi|\right), \tag{31}$$

which is manifestly invariant under rotation and magnetic translation in superspace. Because of this symmetry, the DOS can be reduced to a simple expression involving integrals over two ordinary complex variables. Expressed in terms of two radial and two angular variables, it is

$$\bar{\rho}(E) = \frac{1}{2\pi^2 l_B^2}\,\mathrm{Im}\,\frac{\partial}{\partial\epsilon}\ln\left(\int_0^\infty d(r_1^2/2)\int_0^\infty d(r_2^2/2)\int_0^{2\pi} d\alpha_1 \times\int_0^{2\pi} d\alpha_2\,\exp[i\epsilon(r_1^2+r_2^2) - g_0|r_1^2+r_2^2| - g_3|r_1^2-r_2^2| - 2g_1r_1r_2|\cos(\alpha_1-\alpha_2)| - 2g_2r_1r_2|\sin(\alpha_1-\alpha_2)|]\right). \tag{32}$$

For simplicity, consider the cases where we keep only one of the internode scattering terms, or the random mass term, along with the potential disorder.

(i) For $g_1=g_2=0$, we get

$$\bar{\rho}(E) = \frac{1}{2\pi^2 l_B^2}\left(\frac{g_0}{g_0^2+E^2} + \frac{g_0+g_3}{(g_0+g_3)^2+E^2}\right). \tag{33}$$

(ii) For $g_3=g_2=0$,

$$\bar{\rho}(E) = \frac{1}{2\pi^2 l_B^2}\left(\frac{g_0}{g_0^2+E^2} + \frac{g_0+g_1}{(g_0+g_1)^2+E^2}\right). \tag{34}$$

The answer for the case (iii) $g_3=g_1=0$ is identical to the case (ii). The DOSs obtained for these three cases are identical, as the Hamiltonian involves only one Pauli matrix at a time, and these matrices are related by unitary transformations.

Consider now $g_1=g_2=g_{IN}$ and $g_3=0$. We obtain, defining by I the expression within the large parentheses in Eq. (32),

$$I = -\frac{\pi}{(a^2-2g_{IN}^2)}\left[\pi - 4\frac{g_{IN}}{\sqrt{a^2-g_{IN}^2}}\tan^{-1}\left(\frac{g_{IN}}{\sqrt{a^2-g_{IN}^2}}\right) - 2\sqrt{2}\pi\frac{g_{IN}}{a} + 2\pi\frac{g_{IN}}{\sqrt{a^2-g_{IN}^2}}\right], \tag{35}$$

where $a=g_0-i\epsilon$. The details of the evaluation of the multiple integrals are provided in Appendix A. The expression for the DOS obtained from this expression is lengthy and not very illuminating, but it is important to note that, because of the presence of the term $\tan^{-1}(g_{IN}/\sqrt{a^2-g_{IN}^2})$, we obtain a $\ln E$ divergence at the band center when $g_0=0$. Based on symmetry, similar behavior will be obtained when a combination of two Pauli matrices is considered. This should be contrasted with the $(\ln E)^2$ divergence obtained by Hikami *et al.*[60]

2. $m\neq 0$

When the fermion is massive, we will ignore the mass disorder part. The density of states is given by

$$\bar{\rho}(E) = \frac{1}{2\pi^2 l_B^2}\,\mathrm{Im}\left(\frac{\partial}{\partial\epsilon_1}+\frac{\partial}{\partial\epsilon_2}\right)\ln\left(\int_0^\infty d(r_1^2/2)\int_0^\infty d(r_2^2/2) \times\int_0^{2\pi} d\alpha_1\int_0^{2\pi} d\alpha_2\,\exp[i\epsilon_1 r_1^2 + i\epsilon_2 r_2^2 - g_0|r_1^2+r_2^2| - 2g_1r_1r_2|\cos(\alpha_1-\alpha_2)| - 2g_2r_1r_2|\sin(\alpha_1-\alpha_2)|]\right), \tag{36}$$

where $\epsilon_{1,2}=E\pm m+i\delta$. Again, if we take only one of the internode scattering terms ($g_2=0$) for simplicity, the expression within the large parentheses in Eq. (36), I, becomes

$$I = -\frac{\pi^2}{ab+g_1\sqrt{ab}}. \tag{37}$$

The density of states is then given by

$$\bar{\rho}(E) = \frac{1}{4\pi^2 l_B^2}\sum_{\sigma=\pm1}\frac{g_0}{g_0^2+(E+\sigma m)^2} + \frac{1}{2\pi^2 l_B^2}\frac{g_0[R\cos\beta + g_1\sqrt{R}\cos(\beta/2)] + E[R\sin\beta + g_1\sqrt{R}\sin(\beta/2)]}{R^2+g_1^2R+2g_1R^{3/2}\cos(\beta/2)}, \tag{38}$$

where $R=\sqrt{(g_0^2+m^2-E^2)^2+4g_0^2E^2}$ and $\tan\beta=2g_0E/(g_0^2+m^2-E^2)$. The above expression takes a particularly simple form when $g_0=0$. It becomes

$$\bar{\rho}(E^2 > m^2) = \frac{1}{4\pi^2 l_B^2}\left(\delta(E+m) + \delta(E-m) + \frac{2Eg_1}{(E^2 - m^2 + g_1^2)\sqrt{E^2 - m^2}}\right),$$

$$\bar{\rho}(E^2 < m^2) = 0. \tag{39}$$

If both internode scatterings are present and $g_1 = g_2 = g_{IN}$, the integral is given by

$$I = -\frac{\pi}{(ab - 2g_{IN}^2)}\left[\pi - 4\frac{g_{IN}}{\sqrt{ab - g_{IN}^2}}\tan^{-1}\left(\frac{g_{IN}}{\sqrt{ab - g_{IN}^2}}\right) - 2\sqrt{2}\pi\frac{g_{IN}}{\sqrt{ab}} + 2\pi\frac{g_{IN}}{\sqrt{ab - g_{IN}^2}}\right]. \tag{40}$$

The expression for the DOS is tedious. However, for $g_0 = 0$, the feature that the DOS is zero for $E^2 < m^2$ is still valid. In this case, for energies close to $\pm m$, $\bar{\rho}(E) \sim \ln|E-m|/\sqrt{|E-m|}$.

V. HALL PLATEAU IN THE LOWEST LANDAU LEVEL

Similar to the method described in Ref. 63, we generate the matrix elements of the Dirac Hamiltonian after projecting to the lowest Landau level. In our problem, the element $\langle k|H|k'\rangle$ itself is a 2×2 matrix:

$$\langle k|H|k'\rangle = \int dx\, dy\, \psi_k^*(x,y)[H_{\mathrm{LLL}}^{\mathrm{imp}}(x,y) + m\eta_3]\psi_{k'}(x,y) = m\eta_3\delta_{k,k'} + V(k,k'), \tag{41}$$

where $\psi_k(x,y)$ is the lowest Landau level wave function in the Landau gauge. We choose all the V_j's to follow independent Gaussian white noise distributions such that $\overline{V_j(x,y)V_{j'}(x',y')} = g_j^2\delta_{j,j'}\delta(x-x')\delta(y-y')$. Then the elements of the 2×2 matrix $V(k,k')$ can be computed explicitly—for example,

$$V(k,k')_{11} = \frac{1}{\sqrt{\pi L_y}}e^{-l_B^2(k-k')^2/4}\int d\xi e^{-\xi^2}\left[g_0 u_0\left(l_B\xi + \frac{k+k'}{2}l_B^2, k'-k\right) + g_3 u_3\left(l_B\xi + \frac{k+k'}{2}l_B^2, k'-k\right)\right], \tag{42}$$

where $u_j(x,k)$ is a complex random variable defined to be the Fourier transform of $V_j(x,y)$ along the y direction normalized by the width g_j, namely,

$$u_j(x,k) = \frac{1}{g_j\sqrt{L_y}}\int dy V_j(x,y)e^{iky}. \tag{43}$$

Because each of the disorder fields has zero correlation length, and there are no correlations between them,

$$\overline{u_i(x,k)u_j(x',k')} = \delta_{i,j}\delta(x-x')\delta(k+k'). \tag{44}$$

It is straightforward to compute the statistical properties of the matrix elements. The averages are

$$\overline{V(k,k')_{i,j}} = 0, \quad i,j = 1,2. \tag{45}$$

As to correlations, the only nonvanishing pairs are

$$\overline{V(k_1,k_2)_{11}V(k_3,k_4)_{11}} = \overline{V(k_1,k_2)_{22}V(k_3,k_4)_{22}} = \frac{g_0^2 + g_3^2}{\sqrt{2\pi}L_y}\exp\left(-\frac{l_B^2}{2}[(k_1-k_2)^2 + (k_4-k_1)^2]\right)\delta_{k_1-k_2,k_4-k_3},$$

$$\overline{V(k_1,k_2)_{11}V(k_3,k_4)_{22}} = \overline{V(k_1,k_2)_{22}V(k_3,k_4)_{11}} = \frac{g_0^2 - g_3^2}{\sqrt{2\pi}L_y}\exp\left(-\frac{l_B^2}{2}[(k_1-k_2)^2 + (k_4-k_1)^2]\right)\delta_{k_1-k_2,k_4-k_3},$$

$$\overline{V(k_1,k_2)_{12}V(k_3,k_4)_{12}} = \overline{V(k_1,k_2)_{21}V(k_3,k_4)_{21}} = \frac{g_1^2 - g_2^2}{\sqrt{2\pi}L_y}\exp\left(-\frac{l_B^2}{2}[(k_1-k_2)^2 + (k_4-k_1)^2]\right)\delta_{k_1-k_2,k_4-k_3},$$

$$\overline{V(k_1,k_2)_{12}V(k_3,k_4)_{21}} = \overline{V(k_1,k_2)_{21}V(k_3,k_4)_{12}} = \frac{g_1^2 + g_2^2}{\sqrt{2\pi}L_y}\exp\left(-\frac{l_B^2}{2}[(k_1-k_2)^2 + (k_4-k_1)^2]\right)\delta_{k_1-k_2,k_4-k_3}. \tag{46}$$

For numerical implementation, we discretize and use the integer l to label the x coordinate. We then generate a set of complex random variables $u_j(l,k)$, that are δ correlated as in (44). Finally, we approximate the integrals by sums. Explicitly, the matrix elements are

$$V(k,k+k')_{11} = \frac{e^{-a^2k'^2}}{\sqrt{MA}}\sum_j [g_0u_0(2k+j,k') + g_3u_3(2k+j,k')]e^{-a^2j^2},$$

$$V(k,k+k')_{22} = \frac{e^{-a^2k'^2}}{\sqrt{MA}}\sum_j [g_0u_0(2k+j,k') - g_3u_3(2k+j,k')]e^{-a^2j^2},$$

$$V(k,k+k')_{12} = \frac{e^{-a^2k'^2}}{\sqrt{MA}}\sum_j [g_1u_1(2k+j,k') - ig_2u_2(2k+j,k')]e^{-a^2j^2},$$

$$V(k,k+k')_{21} = \frac{e^{-a^2k'^2}}{\sqrt{MA}}\sum_j [g_1u_1(2k+j,k') + ig_2u_2(2k+j,k')]e^{-a^2j^2}, \tag{47}$$

with $A = \Sigma_j e^{-2a^2j^2}$ and $a^2 = \pi/2M^2$. Here M is the length of

the system in the y direction, the unit being $\sqrt{2\pi}l_B$, that is, $M=L_y/\sqrt{2\pi}l_B$, chosen to be an integer. The integers k and k' label the wave vectors. Since the matrix elements decay exponentially, we can neglect them for $k'>2M$. A cutoff is also necessary for the recursive Green function technique[63] that we use.

We compute the density of states $\rho(E)$ by directly diagonalizing the Hamiltonian. We have checked that $\rho(E)$ is independent of M, for sufficiently large M ($M=32$ seems to be sufficient); the total number of momentum states N_k is chosen to be 1000, which is half the dimension of the Hamiltonian matrix to be diagonalized, as there are two fermions for each k. Typically, an average over 100 disorder realizations is used.

The recursive Green function technique, similar to that in Ref. 63, is used to explore the localization properties. The details are described in Appendix B. We first compute the localization lengths for a finite system, $\lambda_M(E_i)$, at a set of energies, $\{E_i\}_{i=1}^{N_E}$, in systems with transverse dimensions $\{M_j\}_{j=1}^{N_M}$. Since there are two types of fermions, in general there can be two distinct localization lengths; however, in most cases discussed below, they are identical within our numerical accuracy, and we will not generally distinguish them. Assuming finite-size scaling, $\lambda_M(E)/M=f(M^{1/\nu}(E-E_c))$, where $f(x)$ is a universal function, the data are collapsed to obtain the localization length exponent ν and the critical energy E_c. Strictly, scaling holds only for large enough systems in the vicinity of the critical energy. Here the energies $\{E_i\}$ are chosen close to the critical energy E_c, and the validity of the scaling law is verified by the success of the data collapse. For the details of the procedure involving data collapse, see Appendix C.

The numerical calculations about the localization properties were mostly performed for a quasi-one-dimensional system with the transverse dimensions $M=8,16,32,64$. The total number of momentum states is $N_k=5\times10^4$. Because of the 2×2 character of the Hamiltonian matrix elements, the numerical calculations are more demanding than those in Ref. 63. The data are typically averaged over 100 disorder configurations to reduce fluctuations. Energies $\{E_i\}$ were chosen close to the critical energy and measured in units of $2(\Sigma_{j=0}^{3}g_j^2)^{1/2}$, as in Ref. 63.

Our program is also validated by the case $g_0=0.5$, $g_1=g_2=g_3=0$, and $m=0$. In this case, the two types of fermions are independent. Because the LLL wave function is identical to the nonrelativistic one, the properties should be the same as in Ref. 63. Numerical computations show a single peak in the density of states and a localization length exponent of $\nu=2.41\pm0.08$; both agree well with the previous results.

VI. LD TRANSITION FOR THE MASSLESS CASE

A. One disorder field

Consider first the cases where only one type of disorder has nonzero strength. Numerically, we considered (1) $g_3=0.5$, $g_0=g_1=g_2=0$, (2) $g_1=0.5$, $g_0=g_2=g_3=0$, and (3) $g_2=0.5$, $g_0=g_1=g_3=0$. In all of these cases, the δ-function density of states in the pure system is broadened into a simple bell-shape function due to disorder. The results of successful data collapse, not shown here, yield critical exponents $\nu=2.46\pm0.09$, 2.48 ± 0.11, and 2.45 ± 0.08 for cases 1, 2, and 3, respectively, that is, they are the same within the error bars.

The critical exponents are all equal to that of a single type of fermion subject to potential disorder. This can be understood as follows. The original Hamiltonian matrix is in the basis $\{|k_1,1\rangle,|k_1,2\rangle,|k_2,1\rangle,|k_2,2\rangle,\ldots\}$, where 1 and 2 label the type of fermion. If we reorder the basis as $\{|k_1,1\rangle,|k_2,1\rangle,\ldots,|k_1,2\rangle,|k_2,2\rangle,\ldots\}$, the Hamiltonian becomes a 2×2 block matrix with diagonal blocks representing intranode parts, and the off-diagonal blocks representing internode scatterings. Explicitly, it is in the form

$$H=\begin{pmatrix} g_0U_0+g_3U_3+mI & g_1U_1-ig_2U_2 \\ g_1U_1+ig_2U_2 & g_0U_0-g_3U_3-mI \end{pmatrix} \tag{48}$$

where U_i, $i=0,\ldots,3$, are statistically independent random Landau matrices, and I is the identity matrix. The case with only g_3 nonzero has the same structure, and hence the same statistical properties, as the case when only g_0 is nonzero. When only g_1 is nonzero, we can, by a unitary transformation given by

$$T=\mathcal{B}\begin{pmatrix} I & I \\ I & -I \end{pmatrix}, \tag{49}$$

where $\mathcal{B}$ is a normalization constant, bring the Hamiltonian back to the block-diagonal form, resulting in a structure corresponding to two types of independent fermion in the presence of mass disorder. Thus, the critical exponent is the same as the case when only g_0 is nonzero. The same argument also applies to the case when only g_2 is nonzero.

B. Two disorder fields

If one of the two disorder fields is $V_0(x,y)$, and the other is $V_1(x,y)$, or $V_2(x,y)$, or $V_3(x,y)$, an appropriate unitary transformation about an axis by $\pi/2$ will map one possible case to the other. For instance, the transformation in Eq. (49) will transform the case with $V_0(x,y)$ and $V_2(x,y)$ to $V_0(x,y)$ and $V_3(x,y)$. It is therefore sufficient to consider only the case with just $V_0(x,y)$ and $V_3(x,y)$. However, from Eq. (48), the Hamiltonian is block diagonal, and the blocks $g_0U_0+g_3U_3$ and $g_0U_0-g_3U_3$ are statistically equivalent to a new block $\sqrt{g_0^2+g_3^2}U$, with U a new random matrix satisfying the same statistical properties as the U_i's; see Eq. (46). That is, the Hamiltonian for $g_0\neq0$ and $g_3\neq0$ is statistically the same as that corresponding to a potential disorder $\tilde{g}_0=\sqrt{g_0^2+g_3^2}$.

Our numerical computations confirm this argument. The data collapse was found to be successful, assuming $E_c=0$, and the critical exponents are $\nu=2.45\pm0.06$ for $g_0=g_3=0.5$, $g_1=g_2=0$, and $\nu=2.45\pm0.11$ for $g_0=g_1=0.5$, $g_2=g_3=0$.

Next, we choose two disorder fields from $V_1(x,y)$, $V_2(x,y)$, and $V_3(x,y)$. There are three possible combinations. In fact, these three cases are not independent; we can map one case to another by an appropriate unitary transformation corresponding to a rotation by $\pi/2$ about a certain axis.

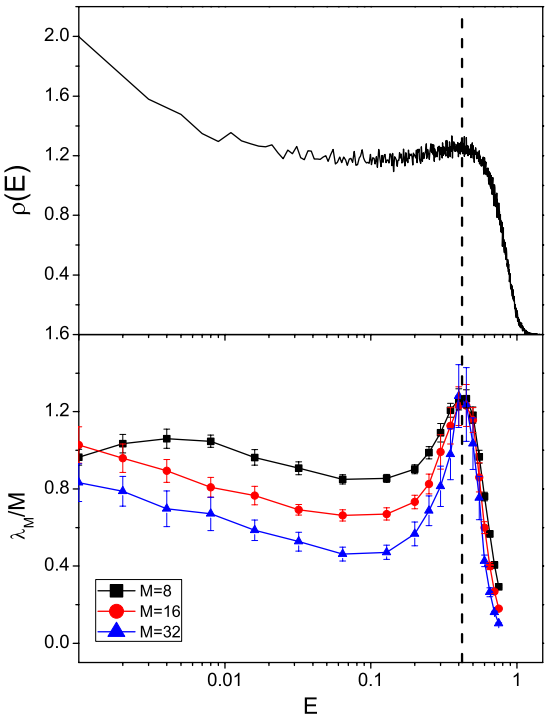

FIG. 1. (Color online) DOS (top) and localization length in finite systems (bottom) for $g_1=g_3=0.5$, $g_0=g_2=0$. The dashed line shows the LD transition.

Therefore, it is sufficient to consider only one of the three cases; for example, let us choose $V_3(x,y)$ (mass disorder), and $V_1(x,y)$ (internode coupling).

We set $g_1=g_3=0.5$, $g_0=g_2=0$. The density of states and the localization lengths are plotted in Fig. 1 for $E>0$; there is symmetry under $E\rightarrow -E$. The extended states are no longer at $E=0$ but shifted to $E=E_c\sim\pm 0.42$. At $E_c\sim\pm 0.42$, we study the localization properties using the data in the range of $|E|>E_c$, since data in the range $|E|<E_c$ are close to both critical points and are likely to lead to inaccurate results. The maximum system size used is $M=64$. Because we do not have *a priori* knowledge of E_c, the statistical procedure discussed in Appendix C is employed to determine E_c and hence the critical exponent ν. The data collapse is shown in Fig. 2. The critical exponent for this parameter set is found to be $\nu=3.23\pm 0.26$, distinct from the nonrelativistic case of $\nu\sim 7/3$.

The present problem can be exactly mapped onto the spin-orbit scattering involving the two-state Landau level problem discussed in Ref. 66; our results are in full agreement. From Fig. 1, there appears to be a divergence in the DOS at the band center, corresponding to a possible LD transition at $E=0$. As shown above, the Cauchy distribution does lead to a $\ln E$ divergence, but such a weak divergence is difficult to detect numerically; note, however, that the numerical calculation involves Gaussian disorder. A semiclassical explanation[67] of the existence of an extended state at the band center for the two-state Landau level problem is known. However, this argument is delicate and fails if a the third kind of disorder is present, which is likely in graphene, where potential disorder cannot be avoided. Thus, we shall not consider further the possible extended state at the band center.

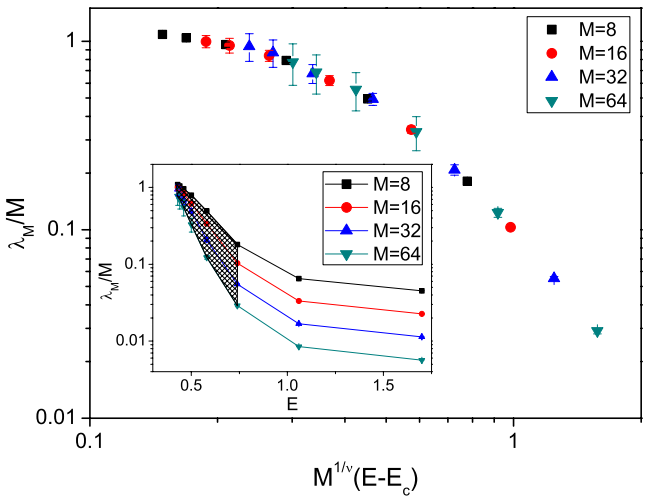

FIG. 2. (Color online) Scaling curve for the case $g_1=g_3=0.5$ and $g_0=g_2=0$. Inset: Dependence of λ_M/M on the energy E for different system sizes M. The shaded area is used for scaling and the critical exponent is found to be $\nu=3.23\pm 0.26$.

It is interesting to study the behavior as the ratio g_1/g_3 is varied. The result for the DOS is shown in Fig. 3. Note that the energy E is in units of $2\sqrt{g_1^2+g_3^2}$. So the extent of the band increases, as g_1 increases. The divergence of the DOS at the band center is a unique feature when g_1 and g_3 are equal, while in the extreme limits there may be a slight dip at $E=0$.

As to ν, a continuously varying exponent is suggested in Fig. 4. In the limit $g_3\gg g_1$ or $g_3\ll g_1$, only one type of disorder dominates; hence the value $\nu\sim 7/3$ is plausible. The

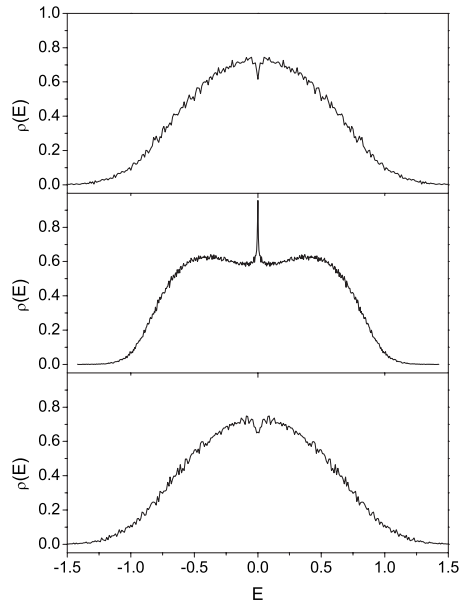

FIG. 3. DOS when mass disorder g_3 and internode coupling g_1 are both present. Parameters are (top) $g_3=10g_1=0.15$; (middle) $g_3=g_1=0.15$; (bottom) $g_3=0.1g_1=0.15$.

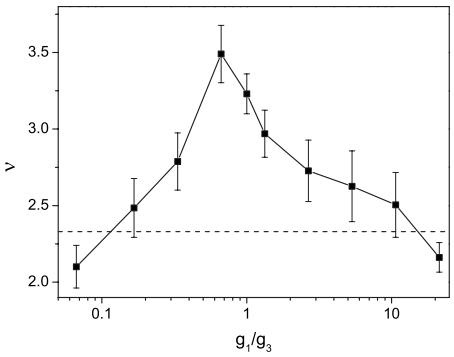

FIG. 4. Dependence of the exponent ν on g_1/g_3. The parameters are $g_0=g_2=0$, $g_3=0.15$, and $m=0$. The dashed line corresponds to $\nu=7/3$.

deviation from this value is largest when $g_1 \sim g_3$, although the data collapse becomes insensitive to the value of ν in the same regime, resulting in larger error. Nonetheless, the results are suggestive of a continuously varying critical exponent.

In the Hamiltonian, the mass disorder $V_3(x,y)$ and the internode scattering disorder $V_1(x,y)$ are accompanied by the Pauli matrices η_3 and η_1. If we apply a unitary transformation

$$T = \mathcal{C}\begin{pmatrix} I & -I \\ I & I \end{pmatrix}, \tag{50}$$

corresponding to a rotation of $\pi/2$ about the y axis, where $\mathcal{C}$ is a normalization factor, the disorder Hamiltonian (48) will be transformed such that $g_3 \to g_1$, $g_1 \to -g_3$. Because we are studying the statistical properties of the system, and all distribution functions are symmetric about zero, the negative sign in front of g_3 is of no importance. This means that this unitary transformation effectively interchanges g_1 and g_3, and hence maps the regime $g_3 > g_1$ to the regime $g_3 < g_1$. Note the symmetry between the two regimes in Figs. 3 and 4.

C. Three disorder fields

The important case in this category is when $g_1 \sim g_2 \sim g_3$; other cases can be roughly understood in terms of the cases discussed above. For numerical computation, we take $g_1 = g_2 = g_3 = 0.5$. The DOS is shown in Fig. 5. Compared to the case when only $g_1 = g_3 = 0.5$, discussed above, the divergence of the DOS at $E=0$ is missing, but the two peaks at $E = \pm 0.46$ survive. This is suggestive of nonexistence of extended states at the band center, but a LD transition at $E \sim \pm 0.46$, which is confirmed by the scaling curve shown in Fig. 6, and a critical exponent of $\nu = 3.6 \pm 0.3$ is obtained. The error bar is large due to a substantial degree of disorder, but the exponent is distinctly different from the value $\nu = 7/3$, indicating a new universality class.

D. Four disorder fields

Finally, we have also examined the case $g_0 \neq 0$, $g_1 \neq 0$. $g_2 \neq 0$, $g_3 \neq 0$. We have found that, when g_0 is small, the potential disorder simply broadens the density of states, and results in a value of ν as though it did not exist; on the other hand a large value of g_0 drives ν to a value close to 7/3.

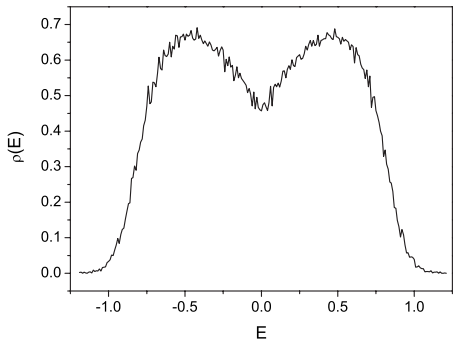

FIG. 5. DOS as a function of energy E in the case $g_1 = g_2 = g_3 = 0.5$, $g_0 = 0$.

VII. LD TRANSITION FOR THE MASSIVE CASE

The constant-mass term results in new physics when combined with the internode coupling, and the resulting phenomena are different from the case when the mass disorder and the internode coupling are combined, as in the previous section.

A. One disorder field

Consider first the case $m \neq 0$ when either g_0 or g_3 is nonzero. From Eq. (48), the random Hamiltonian matrix is block diagonal; hence the two types of nodal fermions are uncoupled. The energies of the two fermions are shifted by the amount of $\pm m$, and the DOS is simply a superposition of two bell-shaped functions centered at $\pm m$. As to localization properties, because the two fermions will have different criti-

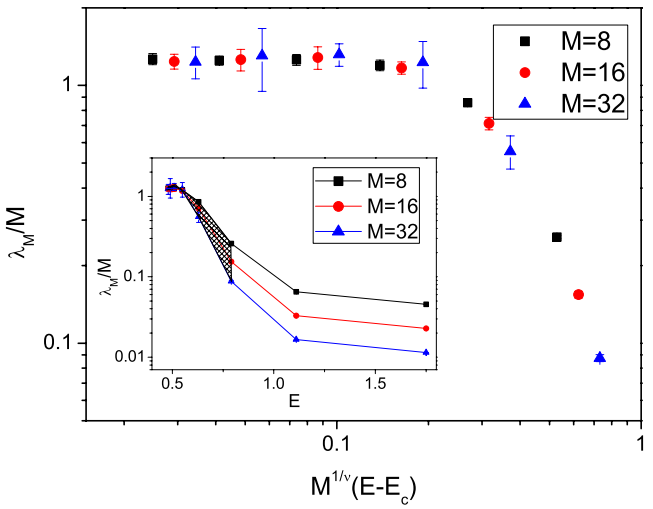

FIG. 6. (Color online) Scaling curve for the case $g_0=0$, and $g_1=g_2=g_3=0.5$. Inset: dependence of λ_M/M on the energy E for different system sizes M. The shaded area is used for scaling. The critical exponent ν is found to be 3.6 ± 0.3.

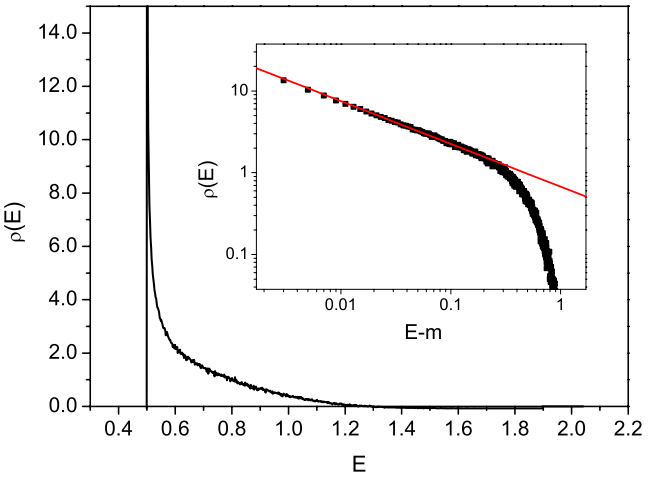

FIG. 7. (Color online) DOS as a function of energy E. In the case $g_0=g_2=g_3=0$, $g_1=0.5$, and $m=0.5$, the DOS vanishes when $|E|<m$. Inset: Logarithmic plot of the DOS around $E=m$, and $m=0.5$. The best fit gives a slope of -0.523 ± 0.003.

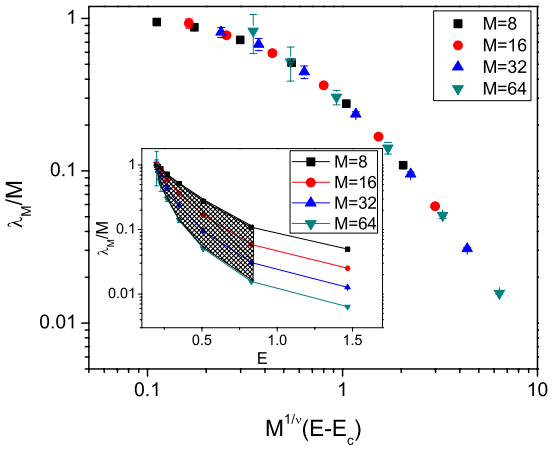

FIG. 8. (Color online) Scaling curve for the case $g_0=g_2=g_3=0$, $g_1=0.4$, and $m=0.15$. Inset: Dependence of λ_M/M on energy E for different system sizes M. The shaded area is used for scaling. Critical exponent is found to be $\nu=1.82\pm0.06$, with the choice of $E_c=m$.

cal energies, namely, $E_c=\pm m$, at a particular energy E these localization lengths will be different from each other. The data collapse for the fermion with $E_c=m$ once again gives a critical exponent of $\nu\sim7/3$.

Consider now finite mass $m\neq0$ and only one internode coupling, for example, $g_1\neq0$. The calculated DOS with $E>0$ region is shown in Fig. 7 for the parameter set $g_0=g_2=g_3=0$, $g_1=0.5$, and $m=0.5$. Qualitatively the results are similar to those of analytical calculations involving the Cauchy distribution, even though the numerical computation is for the Gaussian distribution of disorder. First, the DOS vanishes in the region $|E|<m$. Second, the analytical calculation shows that $\rho(E)\sim(E-m)^{-1/2}$, $E\to m^+$, independent of the value of g_1. The inset of Fig. 7 yields an exponent of -0.523 ± 0.003. We have checked that this value does not vary with g_1, within our numerical accuracy.

As to the LD transition, we perform data collapse with $E_c=m$. The critical exponent turns out to be $\nu=1.82\pm0.06$ for the parameters $g_0=g_2=g_3=0$, $g_1=0.4$, and $m=0.15$ (see Fig. 8), which is significantly different from the usual case corresponding to $\nu\approx7/3$. This striking result implies that the system belongs to a new universality class. We now vary g_1, keeping m fixed to 0.15, and the result for the exponent ν is shown in Fig. 9. It appears that the exponents continuously vary with the ratio g_1/m.

B. Two disorder fields

The most relevant case corresponding to graphene is the one with two types of internode scattering of comparable magnitude. Therefore, we choose $g_1=g_2=m=0.5$. The DOS is shown in Fig. 10. Note that the energy is now measured in units of $2\sqrt{g_1^2+g_2^2}=\sqrt{2}$, so that the divergence is located at $E=m$, which is $m=0.5/\sqrt{2}=0.354$. From the inset in Fig. 10, we find a slope of -0.47 ± 0.01, which is consistent with the analytical result for the Cauchy distribution, namely, $\rho(E)\sim\ln|E-m|/\sqrt{|E-m|}$. Also note the gap in the DOS.

The crossing point in Fig. 10 indicates $E_c\sim0.55$ instead of $E_c=m$. The data collapse is shown in Fig. 11 with a critical exponent of $\nu=3.8\pm0.2$. This critical exponent is not close to any of the values found for a finite mass with a single internode coupling, as in Fig. 9. However, it is reasonably close to the exponent for $m=g_0=g_2=0$ and $g_1\sim g_3$ (see Fig. 4), which is also equivalent to the case $m=g_0=g_3=0$ and $g_1\sim g_2$, as discussed above. Note that $m=0.5$ is much smaller than the bandwidth $2\sqrt{g_1^2+g_2^2}=1.414$, and this critical exponent indicates that the presence of small finite mass will have little effect on the critical exponent as long as two internode couplings are finite.

At the other limit, when m is large enough compared to the bandwidth, the critical exponent $\nu\to1$. Thus, it is reasonable to believe that the exponent also varies continuously, as a function of g_1/m, provided that $g_1=g_2$, and the behavior is similar to that in Fig. 8, except that $\nu\to3.8$ in the limit $m\to0$.

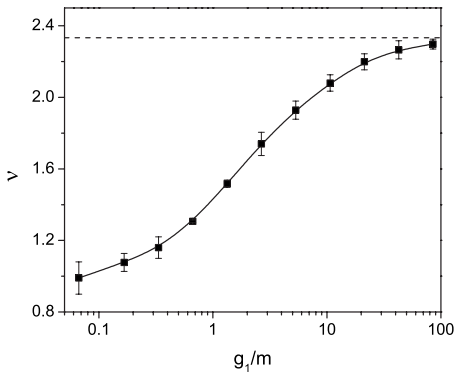

FIG. 9. Dependence of the critical exponent ν on g_1 (normalized by the mass m). The parameters are $g_0=g_2=g_3=0$ and $m=0.15$. The dashed line indicates the level of $\nu=2.33$.

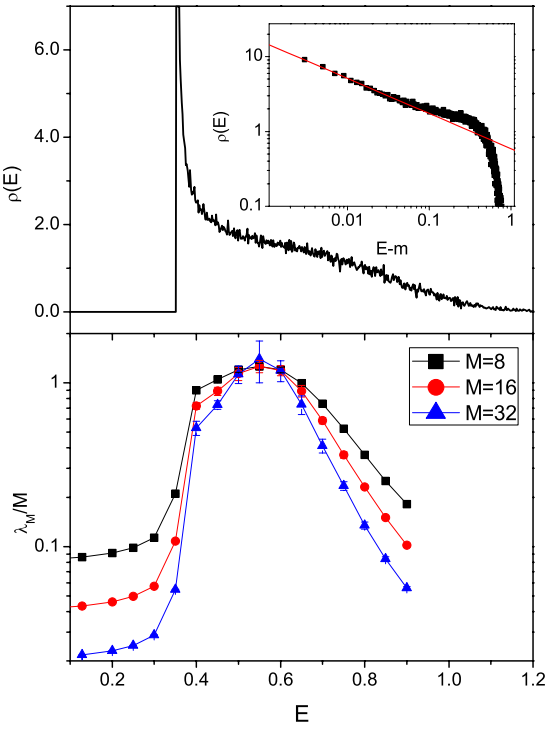

FIG. 10. (Color online) DOS (top) and localization length in finite systems (bottom) for $g_1=g_2=m=0.5$, $g_0=g_3=0$. Inset in top panel: Logarithmic plot of the DOS around $E=m$. The best fit gives a slope of -0.47 ± 0.01.

C. Three disorder fields

Because potential disorder is always present in experiments on graphene, we would like to discuss the case when $g_0\neq 0$, $m\neq 0$, and $g_1=g_2\neq 0$.

First, when m is the smallest parameter, it can be neglected, and hence the massless case discussed above is recovered. Our numerical computations gave a critical exponent of $\nu\sim 3.8$ when $m\ll g_0\ll g_1=g_2$, and $\nu\sim 2.3$ in the limit $m\ll g_1=g_2\ll g_0$, because now the potential disorder is more important than the rest.

When g_0 is the smallest, it will have little effect. Therefore, as discussed in the previous section, there will be a continuously varying exponent from $\nu\sim 1.0$ for $g_0\ll g_1=g_2\ll m$ to $\nu\sim 3.8$ for $g_0\ll m\ll g_1=g_2$.

Finally, if $g_1=g_2$ are smaller than the rest, the internode scattering is no longer important, and hence the two nodal fermions will be decoupled. The exponent will therefore always be $\nu\sim 2.3$ regardless of the relationship between m and g_0.

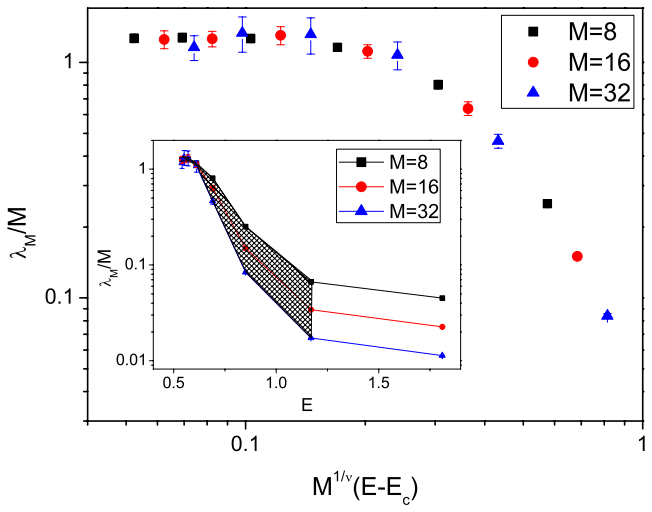

FIG. 11. (Color online) Scaling curve for the case $g_1=g_2=m=0.5$, $g_0=g_3=0$. Inset: Dependence of λ_M/M on the energy E for different system sizes M. The shaded area is used for scaling.

VIII. CONCLUSIONS

We have analyzed the effects of disorder on the LD transition in the LLL of graphene. Because both types of internode scattering, present in the LLL, arise from the random hopping, they will have roughly the same strength. Because the sources of the mass disorder and internode scattering are different, their strengths will be generically different. In some special cases of disorder combinations we have found new universality classes of LD transition in contrast to the conventional IQH.

Our results for the LD transitions in the LLL have direct experimental relevance for the plateau transitions in graphene. Consider first the cases where both the spin and the nodal degeneracies are completely removed. A number of authors have shown that the inclusion of a finite mass and Zeeman energy can explain the appearance of plateaus at $\nu_f=0,\pm 1,\pm 2q$.

Because experiments resolve the spin and nodal splitting, intranode scattering, which always broadens the Landau levels, is weak compared to E_z and m. If the internode scattering strength is larger than the intranode scattering strength, we expect that in the lowest Landau level $0\rightarrow\pm 1$, $1\rightarrow 2$, and $-1\rightarrow -2$ plateau transitions can have different universality classes, in contrast to the conventional IQH effect. In the opposite limit, when the intranode scattering is considerably stronger, the plateau transitions will fall into the conventional IQH universality class with $\nu\sim 2.3$.

For the spin and nodally degenerate plateaus, the potential scattering is strong compared to the Zeeman energy and the mass gap. Theoretically, from our analysis of the massless cases we can infer the plateau transitions to be of the conventional IQH type. However, in experiments, if scaling with respect to the band center is invoked, an effective exponent for these plateau transitions will be observed.

Plateaus at $\nu_f=\pm 4,\pm 6,\ldots$ involve higher Landau levels. In the higher Landau levels, both the random potential at the lattice scale and the random hopping will have nonzero intranode as well as internode scattering contributions. This will complicate the analysis of LD transitions in these levels. Because inclusion of a finite mass does not lift the nodal degeneracies of higher Landau levels, the effect of internode scattering can be strong. In view of the degeneracy factor, there is the possibility of observing an effective exponent for these higher plateau transitions.

ACKNOWLEDGMENT

This work was supported by the NSF under Grant No. DMR-0705092.

APPENDIX A: INTEGRAL

For the Cauchy distribution, in the absence of mass disorder, the calculation of the DOS in Eq. (36) involves the integral

$$I=\frac{1}{4}\int_0^\infty dx\int_0^\infty dy\int_0^{2\pi} d\alpha_1\int_0^{2\pi} d\alpha_2 \exp[-ax-by - 2g_2\sqrt{xy}|\sin(\alpha_1-\alpha_2)|-2g_1\sqrt{xy}|\cos(\alpha_1-\alpha_2)|], \tag{A1}$$

where $a=g_0-i\epsilon_1$ and $b=g_0-i\epsilon_2$. In the massless case $a=b=g_0-i\epsilon$. After performing the integrals over one of the angles, the double integral over the angles is reduced to

$$I_{\rm ang}=8\pi\int_0^{\pi/2} d\alpha_1 \exp[-2\Delta\sqrt{xy}\cos(\alpha_1-\beta)], \tag{A2}$$

where $\Delta=\sqrt{g_1^2+g_2^2}$ and $\tan\beta=g_2/g_1$. Now, expanding the exponential in a power series, integrals over x and y can be easily performed. For the angular integral we use the relation

$$\int_0^{\pi/2} d\alpha_1 \cos^l(\alpha_1-\beta) = -\frac{1}{l+1}\left[\sin^{l+1}\beta\ {}_2F_1\left(\frac{l+1}{2},\frac{1}{2},\frac{3+l}{2},\sin^2\beta\right) + \cos^{l+1}\beta\ {}_2F_1\left(\frac{l+1}{2},\frac{1}{2},\frac{3+l}{2},\cos^2\beta\right)\right], \tag{A3}$$

where ${}_2F_1$ is Gauss's hypergeometric function, and obtain

$$I=-\frac{2\pi}{\Delta ab}\sum_{j=1}^{2}\sum_{l=0}^{\infty}\frac{\Gamma^2[(l/2)+1]}{\Gamma(l+2)}g_j\left(\frac{-2g_j}{\sqrt{ab}}\right)^l \times {}_2F_1\left(\frac{l+1}{2},\frac{1}{2},\frac{3+l}{2},g_j^2/\Delta^2\right). \tag{A4}$$

The summation over l can be performed by the following trick: (1) use the integral representation of ${}_2F_1$, (2) perform a power series summation, which is simple in these cases, and (3) complete the integration over the auxiliary variable introduced for the integral representation. For simplicity we will specialize to the cases (i) $g_1\neq 0, g_2=0$ and (ii) $g_1=g_2=g_{IN}$.

(i) $g_1\neq 0, g_2=0$. In this case we have

$$I=-\frac{2\pi}{ab}\sum_{l=0}^{\infty}\frac{\Gamma^2[(l/2)+1]}{\Gamma(l+2)}\left(\frac{-2g_1}{\sqrt{ab}}\right)^l {}_2F_1\left(\frac{l+1}{2},\frac{1}{2},\frac{3+l}{2},1\right). \tag{A5}$$

We now use the following two relations:

$${}_2F_1\left(\frac{l+1}{2},\frac{1}{2},\frac{3+l}{2},1\right)=\frac{\sqrt{\pi}\Gamma[(3+l)/2]}{\Gamma[(l/2)+1]}, \tag{A6}$$

$$\sum_{l=0}^{\infty}(-x)^l\frac{\Gamma[(l/2)+1]\Gamma[(3+l)/2]}{\Gamma(l+2)}=\frac{\sqrt{\pi}}{2+x}, \tag{A7}$$

to obtain Eq. (37).

(ii) $g_1=g_2=g_{IN}$. In this case we have

$$I=-\frac{2\sqrt{2}\pi}{ab}\sum_{l=0}^{\infty}\frac{\Gamma^2[(l/2)+1]}{\Gamma(l+2)}\left(\frac{-2g_{IN}}{\sqrt{ab}}\right)^l \times {}_2F_1\left(\frac{l+1}{2},\frac{1}{2},\frac{3+l}{2},1/2\right). \tag{A8}$$

Using the integral representation

$${}_2F_1\left(\frac{l+1}{2},\frac{1}{2},\frac{3+l}{2},\frac{1}{2}\right)=\frac{\Gamma[(3+l)/2]}{\Gamma(1/2)\Gamma[(l/2)+1]}\int_0^1 dt\, t^{-1/2}\times\left(\frac{1-t}{1-t/2}\right)^{l/2}\left(1-\frac{t}{2}\right)^{-1/2} \tag{A9}$$

and Eq. (A7), we get

$$I=-\pi\sqrt{2}\sqrt{ab}\int_0^1\frac{dt}{\sqrt{ab}\sqrt{t[1-(t/2)]}+g_{IN}\sqrt{t(1-t)}}. \tag{A10}$$

After performing the integral over t we get Eq. (40). After setting $m=0$ one recovers Eq. (35).

APPENDIX B: RECURSIVE GREEN FUNCTION

Because there are two types of fermion in our problem, the recursive Green function technique is a little more complicated than that introduced by Huckenstein.[63] All the matrix elements, such as those in Eq. (6.9) in Ref. 63, become 2×2 matrices; hence, all the operations, such as multiplication and inversion are matrix operations.

Denote the 2×2 matrix $\langle i|G|j\rangle$ simply by $G(i,j)$. Suppose $G^{(K)}(i,j)$, $i,j=1,\ldots,K$ and, the Green function containing K momentum states is available, then as we add another momentum state, the recursion relations for $G^{(K+1)}(i,j)$ are

$$G^{(K+1)}(K+1,K+1)=\left(E-V(K+1,K+1)-\sum_{i,j}V(i,K+1)^\dagger \times G^{(K)}(i,j)V(j,K+1)\right)^{-1},$$

$$G^{(K+1)}(i,K+1)=\left(\sum_j G^{(K)}(i,j)V(j,K+1)\right) \times G^{(K+1)}(K+1,K+1), \quad i\leqslant K,$$

$$G^{(K+1)}(i,j)=G^{(K)}(i,j)+G^{(K+1)}(i,K+1)G^{(K+1)}(K+1,K+1)^{-1} \times G^{(K+1)}(K+1,j), \quad i,j\leqslant K. \tag{B1}$$

These matrix inversions can be accurately computed because the sizes are small. Corresponding to the two types of fermion, we are interested in $G^{(K)}(1,K)_{n,n}$, $n=1,2$, because the localization length of a system of width M for the nth fermion, $\lambda_{M,n}$, is related to this quantity by

$$\lambda_{M,n}^{-1} = -\frac{M}{K\sqrt{2\pi}l_B}\ln|G^{(K)}(1,K)_{n,n}| = -\frac{M}{K\sqrt{2\pi}l_B}\sum_{k=1}^{K}\ln|q_n^{(K)}|, \tag{B2}$$

where $q_n^{(K)} = G^{(K)}(1,K)_{n,n}/G^{(K-1)}(1,K-1)_{n,n}$. Furthermore, if we define a set of 2×2 matrices $g^{(K)}(j)$, $j=1,\ldots,K$, such that their elements $g^{(K)}(j)_{m,n} = G^{(K)}(1,j)_{m,n}/G^{(K)}(1,K)_{m,m}$, from the recursion relations (B1), we obtain

$$q_n^{(K+1)} = \left[\left(\sum_j g^{(K)}(j)V(j,K+1)\right)G^{(K+1)}(K+1,K+1)\right]_{n,n},$$

$$g^{(K+1)}(i)_{m,n} = \frac{1}{q_m^{(K+1)}}\left[g^{(K)}(i)_{m,n} + \left(\sum_j g^{(K)}(j)V(j,K+1) \times G^{(K+1)}(K+1,i)\right)_{m,n}\right], \quad i \leqslant K,$$

$$g^{(K+1)}(i)_{m,n} = \frac{1}{q_m^{(K+1)}}\left(\sum_j g^{(K)}(j)V(j,K+1) \times G^{(K+1)}(K+1,i)\right)_{m,n}, \quad i = K+1. \tag{B3}$$

APPENDIX C: DATA COLLAPSE

In this appendix, we describe how we can extract the exponent ν, and the critical energy E_c, if necessary, based on the computed localization lengths in finite systems $\lambda_M(E)$ assuming a single-parameter-scaling assumption.

Suppose we have obtained $\{\lambda_M(E)/M\}$ in systems with $\{M_i\}_{i=1}^{N_M}$ for $\{E_j\}_{j=1}^{N_E}$, each with a standard deviation $\{\sigma_{M_i,E_j}\}$. Our goal is to find the proper values of ν and E_c such that all the $N_E\times N_M$ data points collapse onto a single curve:

$$\frac{\lambda_M(E)}{M} = f(M^{1/\nu}(E-E_c)). \tag{C1}$$

Since $f(x)$ is unknown, it is difficult to characterize the quality of the data collapse. To overcome this difficulty, we proceed as follows. Suppose that we are given a pair of values (ν,E_c); we can attempt to represent the unknown function $f(x;\nu,E_c)$ by a polynomial of degree N by simply performing a general fit to Eq. (C2) given below, based on a total of $N_E\times N_M$ data points $\{(x,y,\sigma_y):(\ln[M_j^{1/\nu}(E_i-E_c)], \ln[\lambda_M(E_i)/M_j], \sigma_{M_j,E_i}\}$:

$$\ln\frac{\lambda_M(E)}{M} = \sum_{k=0}^{N} a_k\{\ln[M^{1/\nu}(E-E_c)]\}^k, \tag{C2}$$

where $\{a_i\}_{i=0}^{N}$ are the coefficients to be fitted. In the computer implementation, the order of polynomials was chosen to be $N=5$, since no significant changes were noted by increasing N to 9. The quality of this fit,[64,65] is represented by the variable S defined as

$$S(\nu,E_c) = \sum_{i=1}^{N_E\times N_M}\left(\frac{y_i - f(x_i;\nu,E_c)}{\sigma_i}\right)^2. \tag{C3}$$

If the preset values (ν,E_c) are not correct, the data points will be scattered, resulting in a large value of S, which in turn indicates a poor data collapse. However, when (ν,E_c) attain the correct localization length exponent and the correct critical energy, respectively, S will be minimized. Following this procedure, by minimizing S with the standard gradient descent method, we are able to determine correctly both the critical energy E_c and the localization length exponent ν. Because the scaling law is valid only in the close vicinity of the critical energy, once E_c is obtained from the above procedure, we have to check, for the purpose of self-consistency, that all energies used in the data collapse are indeed close to E_c.

As for the statistical error of ν, the usual procedure is to assume that the minimized $S_{\min}$ follows a χ^2 distribution, and hence the error bar can be drawn corresponding to a certain confidence probability. However, this is not the case in this problem, since $S_{\min}$ does not follow the χ^2 distribution due to the nonlinear form of the estimated parameters ν and E_c in (C2).[65] To draw an error bar for ν statistically correctly, recall that we have the original data $\{(x_i,y_i,\sigma_{y_i})\}$. We generate a large number of data sets synthetically $\{(x_i^{(k)},y_i^{(k)},\sigma_{y_i}^{(k)})\}$, for $k=1,2,\ldots,N_s$, such that $x_i^{(k)}=x_i$, $\sigma_{y_i}^{(k)}=\sigma_{y_i}$, and $y_i^{(k)}$ is a variable randomly distributed in the Gaussian form with a mean of y_i and a standard deviation of σ_{y_i}. Next, we perform exactly the same procedure to get $\nu^{(k)}$ for each synthetic data set $\{(x_i^{(k)},y_i^{(k)},\sigma_{y_i}^{(k)})\}$ as was performed in the actual data set $\{(x_i,y_i,\sigma_{y_i})\}$ for estimating ν and E_c. Finally, the error bar for ν is drawn as the estimated standard deviation

$$\sigma_\nu = \left(\frac{1}{N_s-1}\sum_{k=1}^{N_s}(\nu^{(k)}-\overline{\nu^{(k)}})^2\right)^{1/2}, \tag{C4}$$

where N_s is the number of synthetic data sets and $\overline{\nu^{(k)}}$ is the average of $\nu^{(k)}$. $N_s=10^4$ in computer implementation.

[1] K. S. Novoselov, A. K. Geim, S. V. Morozov, D. Jiang, Y. Zhang, S. V. Dubonos, I. V. Grigorieva, and A. A. Firsov, Science **306**, 666 (2004).

[2] A. Castro Neto, F. Guinea, and N. M. Peres, Phys. World **19** (11), 33 (2006); M. I. Katsnelson and K. S. Novoselov, Solid State Commun. **143**, 3 (2007); A. K. Geim and K. S. Novoselov, Nat. Mater. **6**, 183 (2007).

[3] P. K. Wallace, Phys. Rev. **71**, 622 (1947).

[4] G. W. Semenoff, Phys. Rev. Lett. **53**, 2449 (1984).

[5] M. I. Katsnelson, K. S. Novoselov, and A. K. Geim, Nat. Phys. **2**, 620 (2006).

[6] Y. Zhang, Y.-W. Tan, H. L. Stormer, and P. Kim, Nature (London)

438, 201 (2005).
[7] K. S. Novoselov, A. K. Geim, S. V. Morozov, D. Jiang, M. I. Katsnelson, I. V. Grigorieva, S. V. Dubonos, and A. A. Firsov, Nature (London) **438**, 197 (2005).
[8] Y. Zhang, Z. Jiang, J. P. Small, M. S. Purewal, Y.-W. Tan, M. Fazlollahi, J. D. Chudow, J. A. Jaszczak, H. L. Stormer, and P. Kim, Phys. Rev. Lett. **96**, 136806 (2006).
[9] V. P. Gusynin and S. G. Sharapov, Phys. Rev. Lett. **95**, 146801 (2005).
[10] V. P. Gusynin and S. G. Sharapov, Phys. Rev. B **73**, 245411 (2006).
[11] N. M. R. Peres, F. Guinea, and A. H. Castro Neto, Phys. Rev. B **73**, 125411 (2006).
[12] L. Brey and H. A. Fertig, Phys. Rev. B **73**, 195408 (2006).
[13] D. A. Abanin, P. A. Lee, and L. S. Levitov, Phys. Rev. Lett. **96**, 176803 (2006).
[14] K. Nomura and A. H. MacDonald, Phys. Rev. Lett. **96**, 256602 (2006).
[15] M. O. Goerbig, R. Moessner, and B. Doucot, Phys. Rev. B **74**, 161407(R) (2006).
[16] J. Alicea and M. P. A. Fisher, Phys. Rev. B **74**, 075422 (2006).
[17] V. P. Gusynin, V. A. Miransky, S. G. Sharapov, and I. A. Shovkovy, Phys. Rev. B **74**, 195429 (2006).
[18] I. F. Herbut, Phys. Rev. Lett. **97**, 146401 (2006).
[19] D. V. Khveshchenko, Phys. Rev. B **75**, 153405 (2007).
[20] R. B. Laughlin, Phys. Rev. B **23**, 5632 (1981).
[21] B. I. Halperin, Phys. Rev. B **25**, 2185 (1982).
[22] H. Levine, S. B. Libby, and A. M. M. Pruisken, Phys. Rev. Lett. **51**, 1915 (1983).
[23] A. M. M. Pruisken, Phys. Rev. Lett. **61**, 1297 (1988).
[24] H. Aoki and T. Ando, Phys. Rev. Lett. **54**, 831 (1985).
[25] B. Huckestein and B. Kramer, Phys. Rev. Lett. **64**, 1437 (1990); B. Huckestein, *ibid.* **72**, 1080 (1994).
[26] Y. Huo and R. N. Bhatt, Phys. Rev. Lett. **68**, 1375 (1992).
[27] D. Liu and S. Das Sarma, Mod. Phys. Lett. B **7**, 449 (1993); Phys. Rev. B **49**, 2677 (1994).
[28] J. T. Chalker and P. D. Coddington, J. Phys. C **21**, 2665 (1988).
[29] D. E. Khmel'nitzkii, Pis'ma Zh. Eksp. Teor. Fiz. **38**, 454 (1983) [JETP Lett. **38**, 552 (1983)].
[30] H. P. Wei, D. C. Tsui, M. A. Paalanen, and A. M. M. Pruisken, Phys. Rev. Lett. **61**, 1294 (1988).
[31] S. Koch, R. J. Haug, K. v. Klitzing, and K. Ploog, Phys. Rev. Lett. **67**, 883 (1991).
[32] E. Fradkin, Phys. Rev. B **33**, 3257 (1986); **33**, 3263 (1986).
[33] A. A. Nersesyan, A. M. Tsvelik, and F. Wenger, Phys. Rev. Lett. **72**, 2628 (1994); Nucl. Phys. B **438**, 561 (1995).
[34] A. Altland, B. D. Simons, and M. R. Zirnbauer, Phys. Rep. **359**, 283 (2002), and references therein.
[35] M. P. A. Fisher and E. Fradkin, Nucl. Phys. B **251**, 457 (1985).
[36] A. W. W. Ludwig, M. P. A. Fisher, R. Shankar, and G. Grinstein, Phys. Rev. B **50**, 7526 (1994).
[37] Claudio de C. Chamon, Christopher Mudry, and Xiao-Gang Wen, Phys. Rev. Lett. **77**, 4194 (1996); C. Mudry, S. Ryu, and A. Furusaki, Phys. Rev. B **67**, 064202 (2003).
[38] D. V. Khveshchenko, Phys. Rev. B **75**, 241406(R) (2007); arXiv:0705.4105v2 (unpublished).
[39] D. V. Khveshchenko, Phys. Rev. Lett. **97**, 036802 (2006).
[40] H. Suzuura and T. Ando, Phys. Rev. Lett. **89**, 266603 (2002).
[41] E. McCann, K. Kechedzhi, V. I. Fal'ko, H. Suzuura, T. Ando, and B. L. Altshuler, arXiv:cond-mat/0604015 (unpublished).
[42] K. Nomura and A. H. MacDonald, arXiv:cond-mat/0606589 (unpublished).
[43] S. V. Morozov, K. S. Novoselov, M. I. Katsnelson, F. Schedin, L. A. Pomarenko, D. Jiang, and A. K. Geim, Phys. Rev. Lett. **97**, 016801 (2006).
[44] A. F. Morpurgo and F. Guinea, Phys. Rev. Lett. **97**, 196804 (2006).
[45] D. N. Sheng, L. Sheng, and Z. Y. Weng, Phys. Rev. B **73**, 233406 (2006).
[46] L. Sheng, D. N. Sheng, F. D. M. Haldane, and Leon Balents, arXiv:0706.0371, Phys. Rev. Lett. (to be published).
[47] Y. Zheng and T. Ando, Phys. Rev. B **65**, 245420 (2002).
[48] M. Koshino and T. Ando, Phys. Rev. B **75**, 033412 (2007).
[49] H. P. Wei, S. W. Hwang, D. C. Tsui, and A. M. M. Pruisken, Surf. Sci. **229**, 34 (1990).
[50] S. W. Hwang, H. P. Wei, L. W. Engel, D. C. Tsui, and A. M. M. Pruisken, Phys. Rev. B **48**, 11416 (1993).
[51] L. W. Engel, D. Shahar, C. Kurdak, and D. C. Tsui, Phys. Rev. Lett. **71**, 2638 (1993).
[52] H. P. Wei, L. W. Engel, and D. C. Tsui, Phys. Rev. B **50**, 14609 (1994).
[53] D. K. K. Lee and J. T. Chalker, Phys. Rev. Lett. **72**, 1510 (1994).
[54] D. K. K. Lee, J. T. Chalker, and D. Y. K. Ko, Phys. Rev. B **50**, 5272 (1994).
[55] Z. Wang, D. H. Lee, and X. G. Wen, Phys. Rev. Lett. **72**, 2454 (1994).
[56] C. B. Hanna, D. P. Arovas, K. Mullen, and S. M. Girvin, Phys. Rev. B **52**, 5221 (1995).
[57] V. Kagalovsky, B. Horovitz, and Y. Avishai, Phys. Rev. B **55**, 7761 (1997).
[58] F. Wegner, Z. Phys. B: Condens. Matter **51**, 279 (1983).
[59] E. Brezin, D. J. Gross, and C. Itzykson, Nucl. Phys. B **235**, 24 (1984).
[60] S. Hikami, M. Shirai, and F. Wegner, Nucl. Phys. B **408**, 415 (1993).
[61] V. P. Gusynin, V. A. Miransky, and I. A. Shovkovy, Phys. Rev. D **52**, 4718 (1995).
[62] D. V. Khveshchenko, Phys. Rev. Lett. **87**, 206401 (2001); **87**, 246802 (2001).
[63] B. Huckestein, Rev. Mod. Phys. **67**, 357 (1995).
[64] B. Huckestein, Physica A **167**, 175 (1990).
[65] W. H. Press, S. A. Teukolsky, W. T. Vetterling, and B. P. Flannery, *Numerical Recipes in Fortran 77*, 2nd ed. (Cambridge University Press, Cambridge, UK, 1992), Vol. 1. See Chap. 15.2 for linear fitting and Chap. 15.4 for fitting in polynomial form.
[66] K. Minakuchi and S. Hikami, Phys. Rev. B **53**, 10898 (1996).
[67] D. K. K. Lee, Phys. Rev. B **50**, 7743 (1994).